iScience

CellPress
OPEN ACCESS

Article

Adverse effects of gestational diabetes mellitus on fetal monocytes revealed by single-cell RNA sequencing

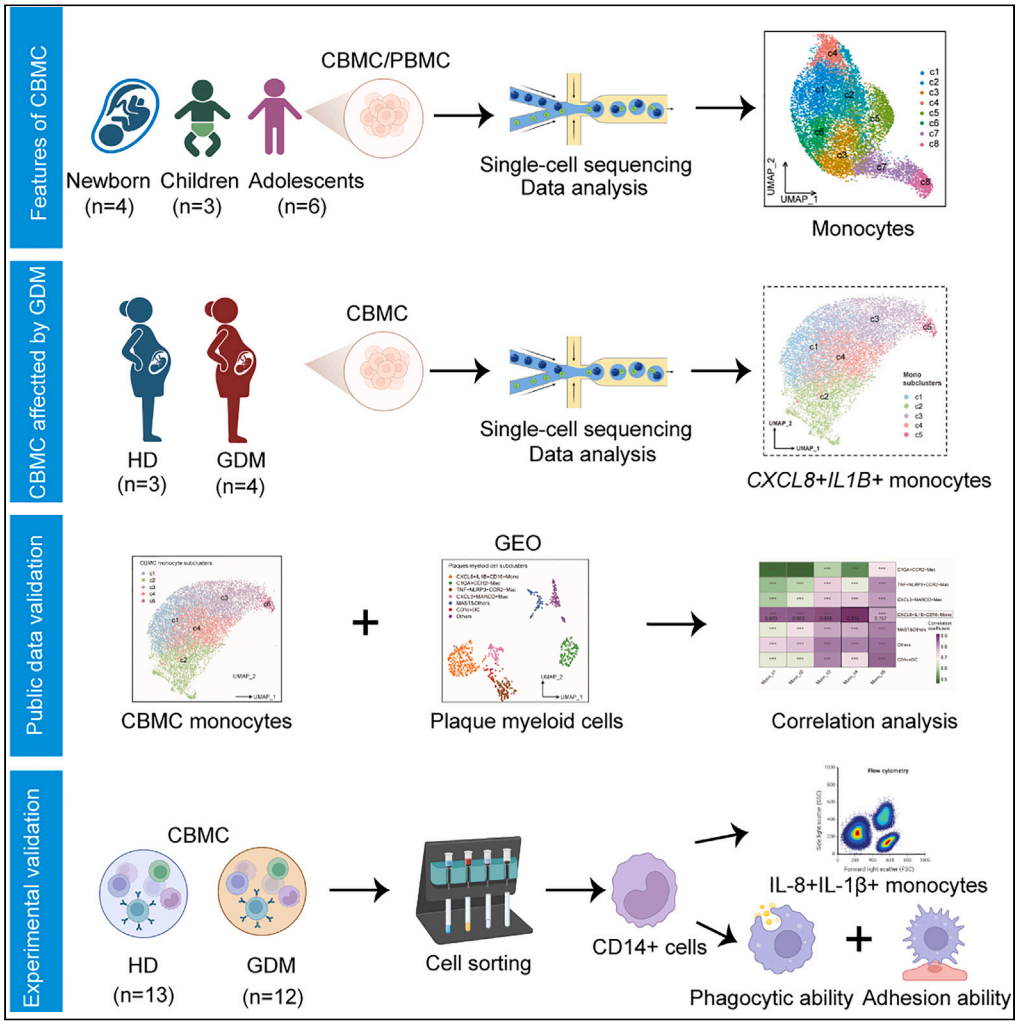

Min Yin, Yan Zhang, Xinyu Li, Shanshan Liu, Juan Huang, Haibo Yu, Xia Li

lixia@csu.edu.cn

Highlights

Cord blood monocytes were characterized by low inflammation and high proliferation

Maternal GDM increased cord blood CXCL8+IL1B+monocytes

Neonatal CXCL8+IL1B+ monocytes share transcriptional traits with plaque myeloid cells

Yin et al., iScience 27, 108637
January 19, 2024
https://doi.org/10.1016/j.isci.2023.108637

iScience

CellPress
OPEN ACCESS

Article

Adverse effects of gestational diabetes mellitus on fetal monocytes revealed by single-cell RNA sequencing

Min Yin,[1,4] Yan Zhang,[1,4] Xinyu Li,[1,4] Shanshan Liu,[1] Juan Huang,[1,2] Haibo Yu,[1,3] and Xia Li[1,5,*]

SUMMARY

Gestational diabetes mellitus (GDM), the most prevalent metabolic disorder during pregnancy, has long-term risks of metabolic diseases in offspring. However, the underlying mechanisms remain unclear. Here, we analyzed single-cell transcriptional data of cord blood mononuclear cells (CBMCs) from fetuses of healthy and GDM mothers, peripheral blood mononuclear cells from children and adolescents, and coronary plaques myeloid cells from atherosclerosis. Our results demonstrated that monocytes in cord blood were characterized with down-regulated proinflammatory-related pathways and up-regulated proliferation-related pathways. And monocytes in cord blood from GDM mothers were featured with expanded CXCL8+IL1B+ subclusters, enhanced crosstalk with neutrophil granulocytes and augmented adhesive and phagocytic abilities. Interestingly, CXCL8+IL1B+ monocytes influenced by GDM had transcriptome similarity with those of coronary plaques myeloid cells from individuals with atherosclerotic cardiovascular disease. Collectively, our data reveal adverse impact of maternal GDM environment on fetal monocytes and propose potential mechanisms between maternal GDM and offspring atherosclerosis.

INTRODUCTION

Diabetes and related metabolic disorders are becoming a global epidemic, with excessive energy intake and a lack of physical activity playing significant roles.[1–3] Besides the above mentioned factors, evidence suggests that metabolic diseases may begin in fetal life, a concept known as the developmental origins of health and disease (DOHaD) theory.[4,5] *In utero* exposure to maternal factors, such as hyperglycemia, obesity, and infection, can reprogram fetuses, leading to negative outcomes that often persist into adulthood, even across generations.[6,7] Therefore, a deeper understanding of DOHaD could be extremely beneficial for the early detection, prevention, and development of new therapeutic approaches for metabolic diseases.

Gestational diabetes mellitus (GDM) is the most prevalent metabolic disease during pregnancy, affecting up to one in every six pregnant women globally.[8] Maternal GDM is closely linked to perinatal complications including preeclampsia, macrosomia, birth injury, neonatal hypoglycemia, and postpartum hemorrhage. More importantly, GDM increases the risk of long-term consequences in their offspring, including diabetes, obesity, and cardiovascular diseases.[9–15] Possible mechanisms include epigenetic deoxyribonucleic acid (DNA) modifications affecting offspring energy balance and metabolism in offspring due to abnormal maternal glucose levels, as suggested by DOHaD theory.[16,17] The emergence of the concept of immunometabolism has expanded our understanding, and mounting evidence indicates that immunity significantly impacts metabolic processes throughout the life cycle.[18] Several studies have shown maternal hyperglycemia altered the immune system in their offspring.[19,20] However, relevant studies are still scarce and the specific mechanisms are not clear. Further research is required to confirm how fetal immune alterations are related to the long-term risk of metabolic diseases.

A few studies have reported that hyperglycemic could promote pro-inflammatory responses of monocytes and also induce trained immunity which might exerting persistent pro-atherogenic effects.[21,22] There are studies demonstrating that this crosstalk between hyperglycemia and monocytes might contribute to obesity and cardiovascular diseases.[18,23] In this sense, maternal fetal-related immune-metabolic reprogramming may play a pivotal role in the pathogenesis of metabolic diseases. However, the crosstalk between maternal metabolic changes and the fetal immune system remains relatively unexplored. Therefore, this study aimed to identify the impacts of maternal GDM on CBMC with transcriptomic analysis at the single-cell level. Our findings indicate that monocytes may play a crucial role in fetal immunity, marked by substantial changes in both proportion and transcription, distinct form the trends observed in childhood and adolescence. Additionally, maternal

[1]National Clinical Research Center for Metabolic Diseases, Key Laboratory of Diabetes Immunology, Ministry of Education, and Department of Metabolism and Endocrinology, The Second Xiangya Hospital of Central South University, Changsha, China
[2]Section of Endocrinology, Department of Internal Medicine, School of Medicine, Yale University, New Haven, CT, USA
[3]Hunan Engineering Research Center of Cell Therapy for Diabetes, Changsha, China
[4]These authors contributed equally
[5]Lead contact
*Correspondence: lixia@csu.edu.cn
https://doi.org/10.1016/j.isci.2023.108637

GDM leads to an abnormal inflammatory state in monocytes and neutrophils. Moreover, *in vitro* experiments have demonstrated that fetal monocytes from CBMC born to mothers with GDM have enhanced phagocytic and adhesive functions. More importantly, a high degree of concordance was found in gene expression when comparing *CXCL8*(IL-8) +*IL1B*(IL-1β) +*FGCR3A*-monocytes from CBMC of mothers with GDM with monocytes from plaques of patients with the coronary syndrome (*CXCL8*+*IL1B* + *FGCR3A*-). Therefore, our single-cell sequencing analysis, *in vitro* functional experiments, and external data validation to investigate how maternal GDM reprograms fetal innate immune cells, providing a potential link between maternal GDM and the increased susceptibility to cardiovascular diseases in the affected offspring. This research might offer some new evidence underlying the DOHaD theory.

RESULTS

Single-cell transcriptomic analysis reveals that fetal monocytes display distinct features

To determine transcriptomic characteristics of neonatal immune cells in single cell dimension, we collected mononuclear cells from umbilical cord blood of three healthy mothers and peripheral blood of three children under the age of 10 for single-cell sequencing. The single-cell transcriptomic data of peripheral blood mononuclear cell (PBMC) from six adolescents aged 10 to 18 was acquired from GEO datasets. Immune cell types were discerned through the utilization of established cell markers (Figures 1A and 1B). Given the exclusive presence of granulocytes in the cord blood data (Figure S1), we excluded this cell type from the comparison to minimize its influence on the proportions of other immune cell types in cord blood. The histograms displayed the differences in immune cell proportions across these three developmental stages (Figure 1C). Results showed that $CD8^+$ cytotoxic T cells and NK cells were scarce in cord blood, but showed a gradual increase with age from birth to adolescence (Figures 1D and 1E). Interestingly, the monocyte population displayed the opposite trend, as it manifested a notable age-related decline (Figure 1F), and it held the second-highest proportion (27.9%) in umbilical cord blood (Figure 1C), underscoring their potential significance in fetal immunity. Furthermore, the differential analysis of immune cells revealed that, in comparison to childhood and adolescence, cord blood monocytes exhibited the highest number of differentially expressed genes (DEGs) (Figure 1G). PALMO analysis revealed that the expression levels of pro-inflammatory factors, such as *IL1B* and *CXCL8*, were comparatively lower in umbilical cord blood mononuclear cells (CBMCs), while the expressions of anti-inflammatory factors, such as *TGFB1* and *TGFA*, were notably higher (Figure 1H). These findings suggest that monocytes may play a crucial role in fetal immunity, characterized by substantial changes in both proportion and transcription, distinct from the patterns observed in childhood and adolescence.

Transcriptome analysis reveals functional characteristics of cord blood monocytes

To gain further insight into the subtype and functional characteristics of monocytes in cord blood, we conducted unsupervised clustering analysis, which allowed us to categorize monocytes into eight subgroups (Figure 2A). Based on the expression levels of *CD14* and *FCGR3A*(CD16), clusters c1 to c6 were classified as classical monocytes, whereas cluster c8 represented non-classical monocytes and c7 represented intermediate monocytes (Figure 2B). The proportion of c8 was the lowest in cord blood, and increased rapidly with age (Figure 2C). For classical monocytes clusters, we examined their characteristics and age-dependent patterns (Figures 2D and 2E). Clusters c1(*RBP7*+), c3 (*RACK1*+) and c6 (*S100A9*+) displayed a noticeable decrease with age, whereas cluster c4 (*IL1B* + *CXCL8*+) exhibited a rapid increase with age (Figure 2D). Moreover, an additional AUCell analysis indicated that cluster c1 appeared to be relatively quiescent, c3 exhibited higher expression of proliferation-related pathways, c6 had a higher expression of several metabolic processes, while c4 showed enrichment in TNFA signaling pathways (Figure 2F).

To explore the developmental stages of each cluster, we employed CytoTRACE for cell developmental trajectory analysis (Figure 2H). To ensure a focused examination of the evolution process between subpopulations and to mitigate the influence of a wide age range, we initially relied solely on cord blood data for prediction (Figures 2G–2I). Genes that most corelated with CytoTRACE were shown in Figure 2J. The CytoTRACE analysis unveiled that cluster c3 primarily resided in the early stage of the pseudo-time axis (indicating a less differentiated state), while nearly all cells in cluster c4 were positioned at the terminal end of the axis (indicating a more differentiated state) (Figures 2G–2I). These results remained consistent when examined in children and adolescents (Figure S2A–S2F) and the trajectories were superimposed onto the UMAP (Figure S2G). In summary, monocytes in cord blood exhibit a greater prevalence of naive and highly proliferative subsets, alongside a reduced proportion of pro-inflammatory subsets expressing inflammatory factors.

Cord blood monocytes from GDM mothers are characterized by an elevation in subcluster marked by *IL1B* and *CXCL8*

GDM stands as a prevalent complication during the perinatal period, and our analysis hints at the pivotal role that monocytes might play in fetal development. To delve deeper into the influence of maternal GDM on fetal monocytes, we conducted single-cell sequencing using cord blood samples collected from four mothers with GDM and three healthy mothers (Figure S3). The clinical and laboratory data of these 7 individuals were summarized in Tables S1–S3. We found no significant difference in the proportion of immune cells between the two groups (Figure S3). To differentiate monocyte clusters with higher resolution, we conducted an unsupervised clustering analysis, which led to the subdivision of monocytes into five distinct subclusters (Mono c1 - c5). These subclusters were annotated based on specifically expressed marker genes and cell surface protein expression levels (Figures 3A–3C). The *FCGR3A*-classical monocytes were further classified into resting monocytes (Mono c1-c2) and pro-inflammatory monocytes (Mono c3-c4) based on their expression levels of *IL1B* and *CXCL8*, while cluster 5 (Mono c5) represented *FCGR3A*+ non-classical monocytes. Notably, Mono c4 exhibited high expression of *IL1B* and *CXCL8*, suggesting it may have the most pro-inflammatory effect (Figure 3C). In the GDM group, the proportion of Mono c4 within

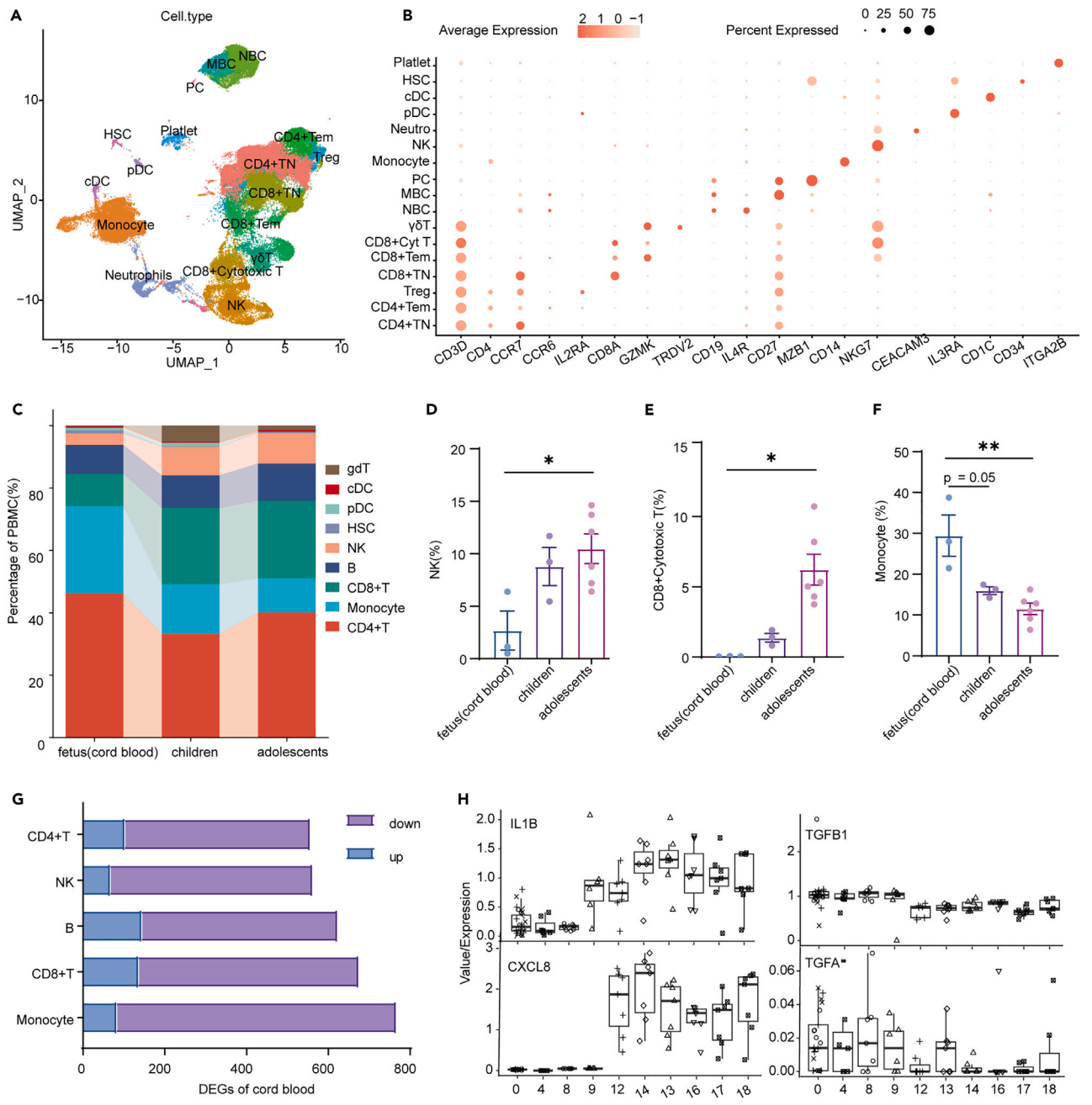

Figure 1. Characteristics of immune cells in cord blood

(A) UMAP projection of mononuclear cells clustered by gene expression patterns.

(B) The marker genes used to identify each type of immune cell. The color depth represents the expression level, and the dot size represents the expression proportion (unit: %).

(C) The proportion of peripheral immune cell subsets in cord blood (left), children (middle) and adolescents (right).

(D–F) The proportion of immune cells in different groups. (D) NK; (E) CD8+Cytotoxic T; (F) Monocyte.

(G) Histogram of the number of up-regulated and down-regulated differently expressed genes (DEGs) in major immune cells of umbilical blood, compared with childhood and adolescence. DEGs were ranked by average log2 (fold change) after filtering with a minimum |log2(fold change) | of 0.585 and a maximum FDR (q-value) of 0.05.

(H) PALMO was used to calculate the expression changes of representative pro-inflammatory genes (left) and anti-inflammatory genes (right) in monocytes with age. The horizontal axis represents age (years), the vertical axis represents average expression levels (counts), and the dots represent the average expression levels of this gene in the original Seurat subpopulation belonging to monocytes in each sample. Data were tested by independent sample t-test, and were represented as mean ± SEM.* means the p value of correlation analysis is <0.05. ** means the p value of correlation analysis is <0.01.

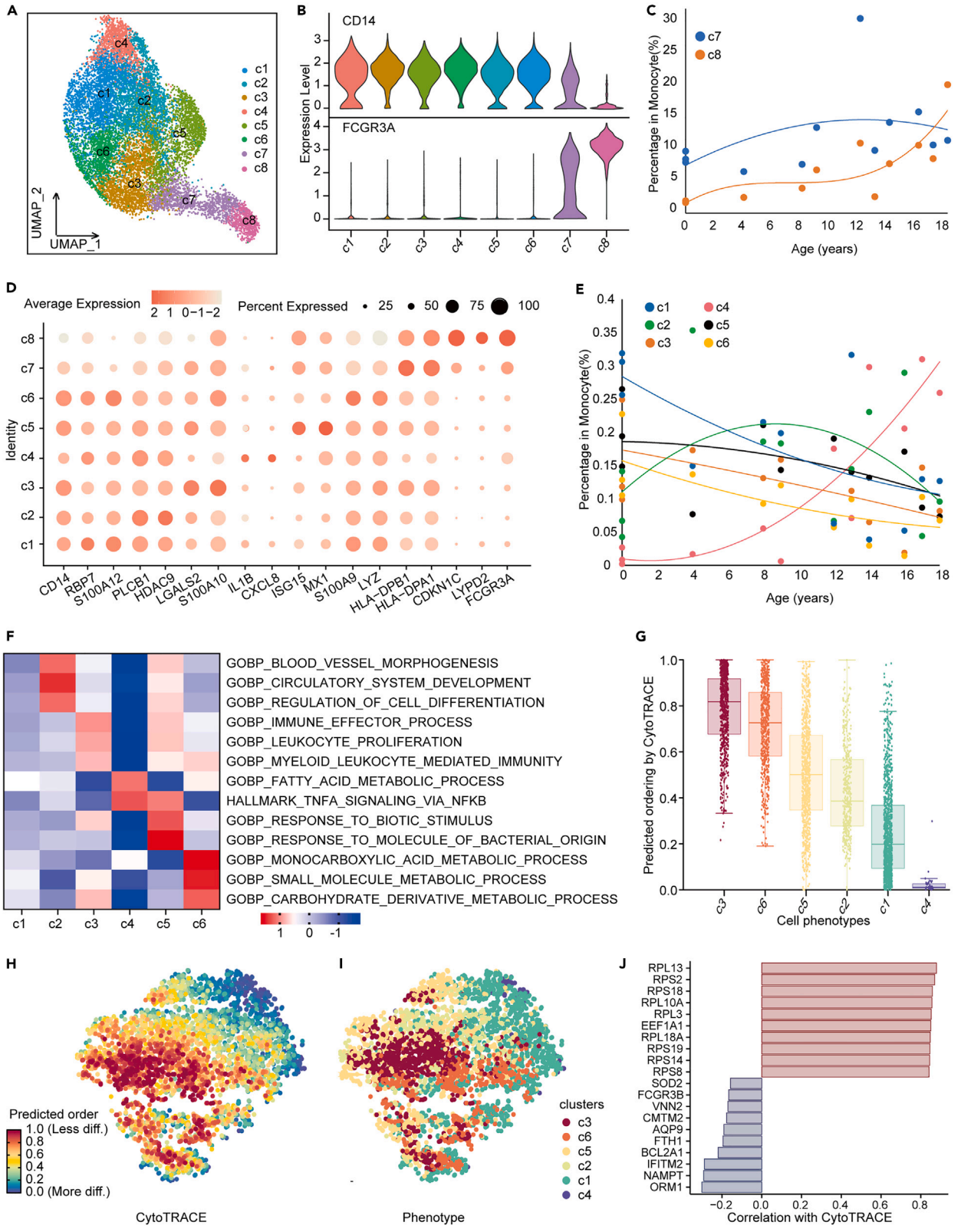
A
c1
c2
c3
c4
c5
c6
c7
c8
UMAP_1
UMAP_2
B
CD14
FCGR3A
Expression Level
C
Percentage in Monocyte(%)
Age (years)
D
Average Expression
Percent Expressed
Identity
CD14
RBP7
S100A12
PLCB1
HDAC9
LGALS2
S100A10
IL1B
CXCL8
ISG15
MX1
S100A9
LYZ
HLA-DPB1
HLA-DPA1
CDKN1C
LYPD2
FCGR3A
E
Percentage in Monocyte(%)
Age (years)
F
GOBP_BLOOD_VESSEL_MORPHOGENESIS
GOBP_CIRCULATORY_SYSTEM_DEVELOPMENT
GOBP_REGULATION_OF_CELL_DIFFERENTIATION
GOBP_IMMUNE_EFFECTOR_PROCESS
GOBP_LEUKOCYTE_PROLIFERATION
GOBP_MYELOID_LEUKOCYTE_MEDIATED_IMMUNITY
GOBP_FATTY_ACID_METABOLIC_PROCESS
HALLMARK_TNFA_SIGNALING_VIA_NFKB
GOBP_RESPONSE_TO_BIOTIC_STIMULUS
GOBP_RESPONSE_TO_MOLECULE_OF_BACTERIAL_ORIGIN
GOBP_MONOCARBOXYLIC_ACID_METABOLIC_PROCESS
GOBP_SMALL_MOLECULE_METABOLIC_PROCESS
GOBP_CARBOHYDRATE_DERIVATIVE_METABOLIC_PROCESS
G
Predicted ordering by CytoTRACE
Cell phenotypes
H
Predicted order
1.0 (Less diff.)
0.0 (More diff.)
CytoTRACE
I
clusters
Phenotype
J
RPL13
RPS2
RPS18
RPL10A
RPL3
EEF1A1
RPL18A
RPS19
RPS14
RPS8
SOD2
FCGR3B
VNN2
CMTM2
AQP9
FTH1
BCL2A1
IFITM2
NAMPT
ORM1
Correlation with CytoTRACE

Figure 2. Cell composition characteristics of monocytes in umbilical cord blood

(A) UMAP projection of monocyte cells clustered by gene expression patterns.

(B) The violin diagrams display the expression of CD14 and FCGR3A in subclusters of monocytes.

(C) The proportion of intermediate monocytes (c7) and non-classical monocytes (c8) changed with age. Points represent each sample. Quadratic regression was used for fitting.

(D) The marker gene used to identify each cluster of monocytes. The color depth represents the expression level, and the dot size represents the expression proportion (unit: %).

(E) The proportion of classical monocytes (c1-c6) changed with age. Points represent each sample. Quadratic regression was used for fitting.

(F) AUCell analysis results of monocyte subclusters. The color represents the AUCell score. When the score is higher, we predicted higher the pathway activation in the cluster.

(G) Boxplot showed the predicted ordering by CytoTRACE. The vertical axis represented the ordering score, and the higher the score, the lower the differentiation degree of the cell.

(H) TSNE plot displayed the predicted ordering of classical monocytes (c1-c6) by CytoTRACE. The color represented the ordering score.

(I) TSNE projection of classical monocytes (c1-c6) clusters. The colors represented different clusters.

(J) Top 20 genes that most affect the predicted ordering of CytoTRACE.

the total monocytes accounted for 27%, which marked a noteworthy increase in comparison to 19% in the healthy group (Figure 3D). Considering that the immunophenotype and functional characteristics of c2 closely resembled a non-inflammatory or resting state, we also calculated the ratio of the numbers of c4 and c2 clusters. We found the ratio of the numbers of c4 and c2 increased in GDM group (Figure 3E), although statistical significance within the GDM group was not reached ($p = 0.087$). In addition, AUCell analysis further emphasized that Mono c4 in the GDM group was predominantly enriched in pro-inflammatory pathways, such as the inflammatory response, IFN-I signaling, defense response, TNF-α, and NF-κB signaling pathways. Furthermore, lipid and cell adhesion pathways exhibited upregulation in Mono c4 from the GDM group (Figures 3F and 3G).

Despite Mono c3 and c5 also displaying immune and inflammatory activation, their proportions remained relatively consistent between the two groups. Collectively, GDM affects umbilical cord blood monocytes, characterized by an increase in *IL1B + CXCL8+* monocytes. These findings suggested that the balance between inflammatory and resting clusters in GDM monocytes is disrupted.

To validate the aforementioned impact of GDM on monocyte phenotype and function, we collected umbilical cord blood samples from 12 mothers with GDM and 13 age-matched healthy mothers. The clinical and laboratory data for these 25 individuals were summarized in Tables S4–S6. Flow cytometric analysis confirmed a significant increase in the proportion of IL-8+IL-1β+ cells in monocytes within the monocytes of the GDM group, rising from 20% to nearly 40% (Figure 4A). Notably, the proportion of IL-8+IL-1β+ monocytes showed a positive correlation with maternal peak blood glucose levels (oral glucose tolerance test at 60 min (OGTT-60 min)) and the incremental value of blood glucose between OGTT-60 min and fasting blood glucose during pregnancy (Figure 4B). *In vitro* experiments further substantiated these findings, as both the proportion of IL-8+IL-1β+ cells and the mean fluorescent intensity (MFI) of IL-8 and IL-1β in CBMC were significantly stimulated by high glucose levels, in the presence or absence of lipopolysaccharides (LPS) (Figure 4C). This suggests that hyperglycemia may activate the expression of inflammatory cytokines in monocytes. Moreover, additional functional experimental results confirmed that monocytes from the GDM group exhibited enhanced lipid phagocytosis (Figure 4D) and improved endothelial adhesion function (Figure 4E) compared to the control group. In summary, these findings collectively indicate an increase in the proportion of *IL1B + CXCL8+* monocytes in umbilical cord blood of GDM offspring, alongside enhanced lipid phagocytosis and adhesion functions.

Cord blood granulocytes from GDM mothers exhibited an increase in *CXCL8+FCGR3B +* neutrophils

The findings presented above indicates that GDM induces a pro-inflammatory phenotype in monocytes of offspring. Consequently, we proceeded to analyze other cell types in cord blood and observed a similar impact of maternal GDM on neonatal neutrophils. Among fetal CBMC, granulocytes were a prominent cell type, and we identified eight subclusters through unsupervised cluster analysis ((Figure 5A). In line with the monocyte results, *CXCL8+FCGR3B +* neutrophils (c1) displayed a marked increase in the GDM group (Figures 5B and 5C), while granulocyte subclusters with high *ELANE* and *MPO* expression (c3 and c6) exhibited a decreasing trend in the GDM group (Figures 5D and 5E). Notably, apart from the increased proportion, *CXCL8+FCGR3B +* neutrophils (c1) from the GDM group also exhibited higher levels of *CXCL8* expression compared to the healthy group (Figure 5F). Furthermore, these *CXCL8+FCGR3B +* neutrophils (c1) showed enrichment in pro-inflammatory transcriptional signatures, including genes associated with TNF-α, NF-κB, and chemokine signaling pathways. In contrast, pathways related to the defense response to bacteria and oxidative phosphorylation were suppressed in *CXCL8+FCGR3B +* cells in the GDM group (Figures 5G–5O). In summary, the granulocytes exhibited an expansion of *CXCL8+FCGR3B +* cluster in the GDM group, which had inflammatory transcriptional signatures.

Monocytes and neutrophils from the maternal GDM group exhibited enhanced crosstalk in inflammatory signaling pathways

Given the alterations observed in monocytes and neutrophils of GDM offspring, we examined the cell-cell interactions between these two cell types. Cell-cell communication analysis revealed that *CXCL8+FCGR3B +* neutrophils exhibited the highest probability of engaging in intercellular communication with monocytes. Furthermore, among these intercellular communication signals, Mono c3 and Mono c4 displayed the highest probability of communicating with granulocytes (Figures 6A and 6B). More importantly, GDM-specific clusters highlighted the unique

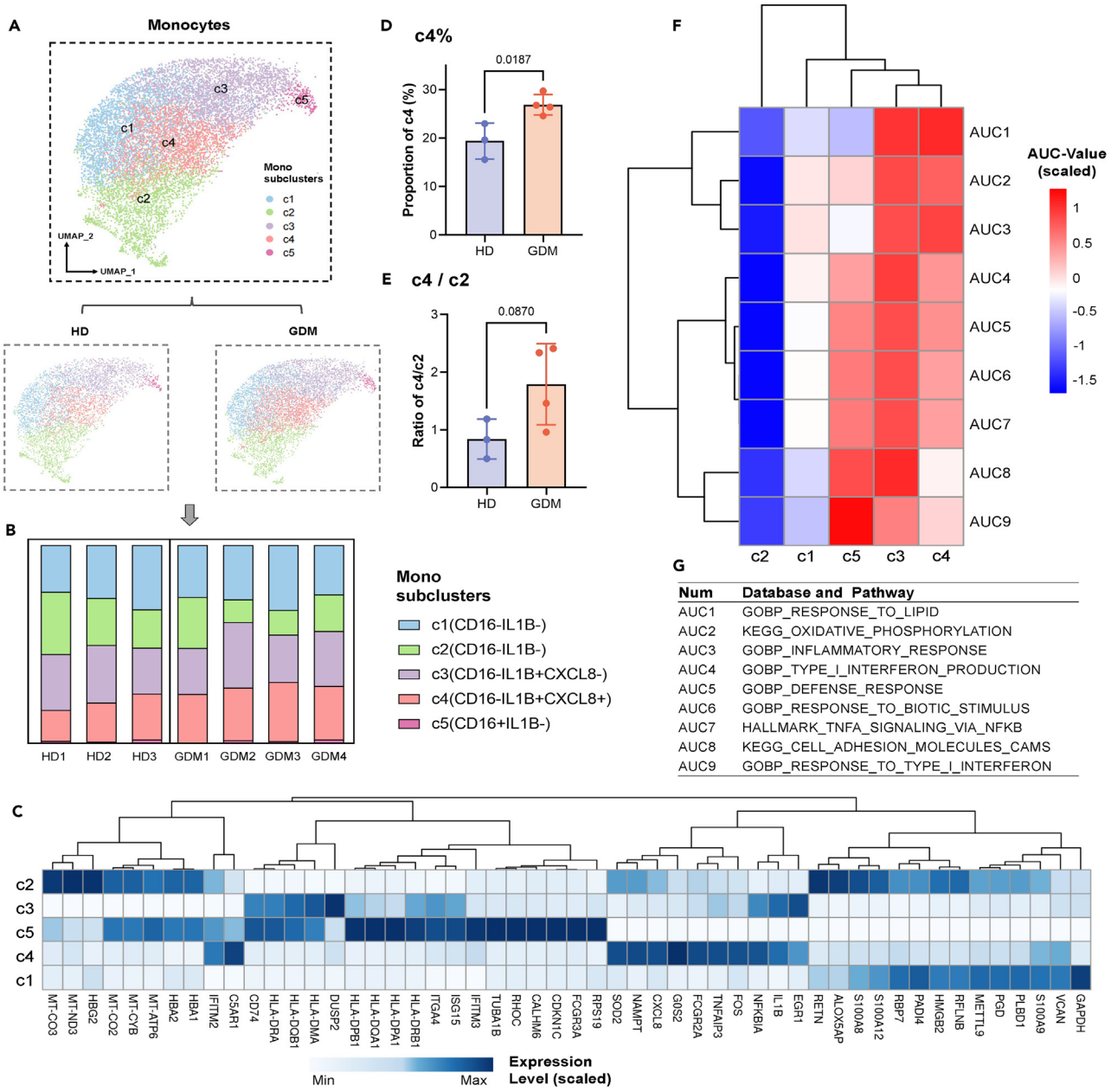

Figure 3. Identification of CBMC monocyte subclusters and their pro-inflammatory effects in the GDM group

(A) UMAP plots of monocyte subclusters in HD (lower left), GDM (lower right) and merge of them (upper).

(B) Pileup bar plot depicts the cell abundance of each monocyte subcluster.

(C) Heatmap shows the scaled mean expression of differential genes in each subcluster. The clustering analysis was applied to the gene markers of the columns.

(D) The comparison of c4 proportion between two groups in monocytes.

(E) The comparison of the ratio of c4 and c2 subclusters between two groups in monocytes.

(F) Heatmap represents the scaled mean AUC values of differential signaling pathways in each subcluster. The clustering algorithm was applied to the row and column variables.

(G) Database and pathway names corresponding to each AUC number. All data were tested by independent sample t-test, and were represented as mean ± SD.

interactions. When *CXCL8+FCGR3B +* neutrophils acted as providers of ligands, they showed specific elevated levels of communication with *CXCL8+IL1B +* monocytes through CCL3-5 signaling (Figure 6A). Conversely, when ligands were provided to *CXCL8+IL1B +* monocytes, the communication levels of CCL3-5 and CXCL8 signals were specifically upregulated (Figure 6B).

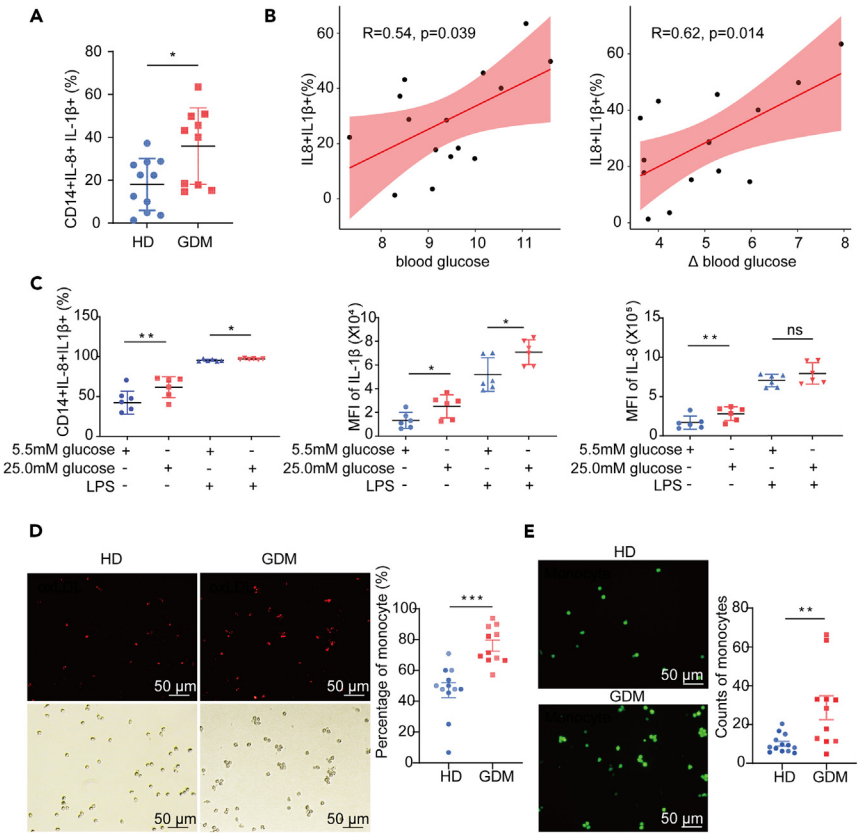

Figure 4. Validation of IL-8+IL-1β+ monocyte expansion and pro-inflammatory effects *in vitro*

(A) The proportion of IL-8+IL-1β+ cells in the $CD14^+$ monocytes from the GDM or HD group (GDM: HD = 11:13, 3 samples with low cell viability were removed).

(B) Correlation between the proportion of IL-8+IL-1β+ monocytes and blood glucose during OGTT (n = 15).

(C) The inflammatory phenotype proportion and cytokine MFI under different glucose concentrations (5.5 mM or 25 mM), LPS interventions, or both (n = 6).

(D) The proportion of monocytes participating in lipid phagocytosis (GDM: HD = 11:13, one sample with low cell viability was removed). Dil-oxLDL (red fluorescence) was utilized to assess monocyte phagocytosis.

(E) The proportion of monocytes participating in endothelial adhesion was labeled with CFSE reagent (green fluorescence) (GDM: HD = 11:13). All data were tested by independent sample t-test, and were represented as mean ± SEM.* means the p value of correlation analysis is <0.05. ** means the p value of correlation analysis is <0.01. *** means the p value of correlation analysis is <0.001.

Signaling networks of IL1, IL4, IL6, IL15, LTA, and CCL were enhanced in the GDM group when comparing the signaling weights between the two groups (Figure 6C). Most of these upregulated pro-inflammatory communications involved *CXCL8+FCGR3B* + neutrophils, Mono c1, c3, and *CXCL8+IL1B* + monocytes. While Mono c1 and c3 did not increase in GDM compared to the HD, their communication of pro-inflammatory signals with *CXCL8+FCGR3B* + neutrophils did. Conversely, a deficiency of anti-inflammatory TGF-β signaling was detected in the GDM group, especially in *CXCL8+FCGR3B* + neutrophils (Figure 6C). These findings suggest that *CXCL8+IL1B* + monocytes and *CXCL8+FCGR3B* + neutrophils engage in a complex dialogue during the maternal-fetal reprogramming process influenced by maternal GDM.

Pro-inflammatory monocytes of cord blood share transcriptional characteristics similar to myeloid cells in coronary culprit plaques

Considering the increased risk of arteriosclerosis in GDM offspring, coupled with the knowledge that pathogenic macrophages in arterial plaques primarily originate from the bloodstream, we investigated an investigation to explore the association between the pro-inflammatory CBMC cluster and pathogenic cell populations within atherosclerotic plaques. We first analyzed the *IL1B* and *CXCL8* expression patterns of peripheral blood monocytes at different stages of coronary artery disease (CAD) utilizing publicly available transcriptome sequencing dataset. An enrichment of IL1B and CXCL8 expression in the acute myocardial infarction group when compared to the normal coronary angiography group was present. Furthermore, transcriptional similarities between expanded monocytes in GDM offspring and myeloid cells present in coronary culprit plaques (dataset from GEO: GSE184073) on the single-cell level were explored. By referring to marker genes provided by the original authors, we annotated the types of myeloid cells within the plaques (Figure 7C). As demonstrated in Figure 7F, the proportion of monocyte clusters in vulnerable plaques was significantly higher than that in stable plaques in patients with chronic coronary syndrome (CCS), indicating the potential roles

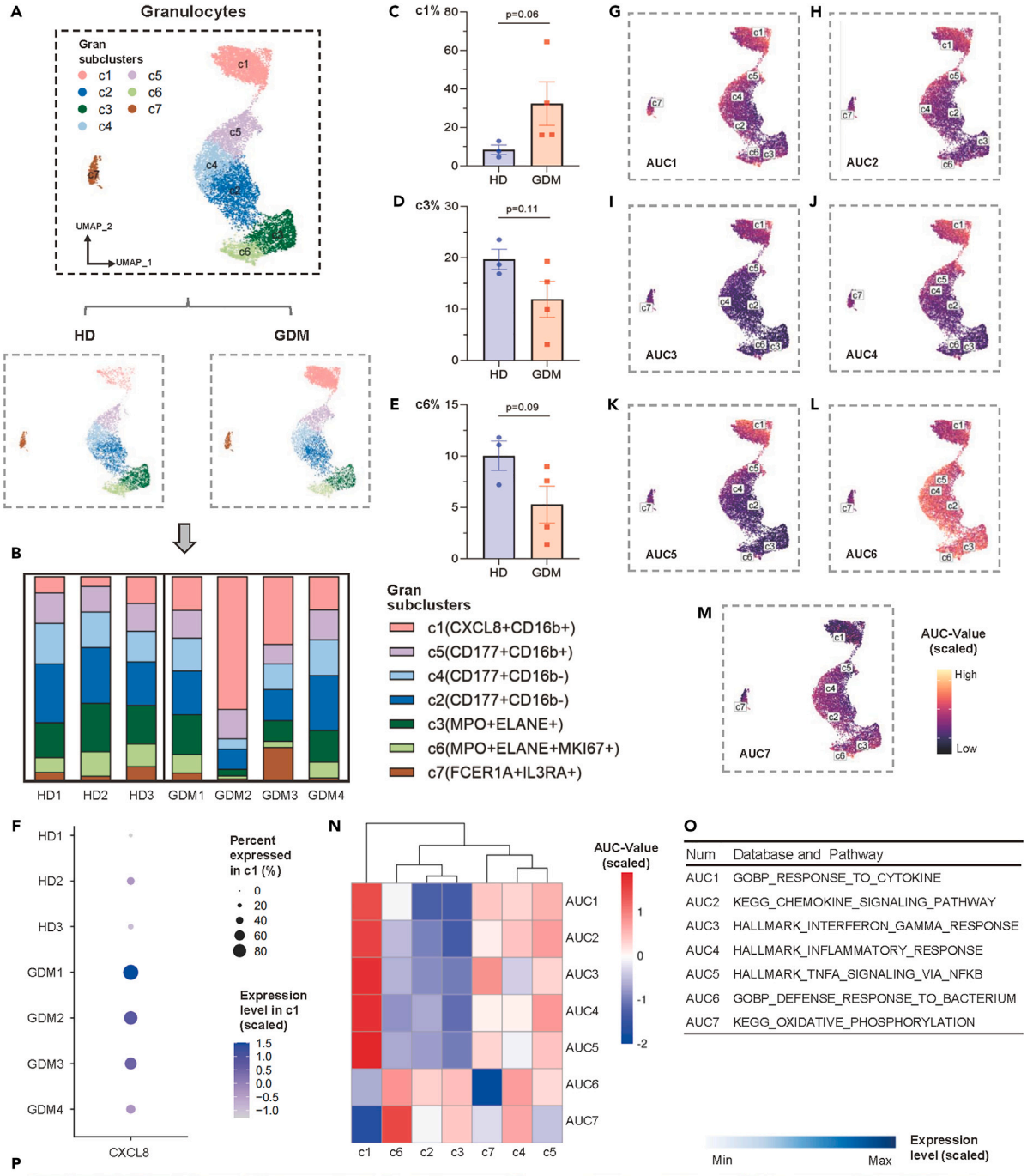

Num	Database and Pathway
AUC1	GOBP_RESPONSE_TO_CYTOKINE
AUC2	KEGG_CHEMOKINE_SIGNALING_PATHWAY
AUC3	HALLMARK_INTERFERON_GAMMA_RESPONSE
AUC4	HALLMARK_INFLAMMATORY_RESPONSE
AUC5	HALLMARK_TNFA_SIGNALING_VIA_NFKB
AUC6	GOBP_DEFENSE_RESPONSE_TO_BACTERIUM
AUC7	KEGG_OXIDATIVE_PHOSPHORYLATION

Figure 5. Identification of CBMC granulocyte subclusters and their pro-inflammatory effects in the GDM group

(A) UMAP plots of granulocyte subclusters in HD (lower left), GDM (lower right), and the merge of them (upper).

(B) Pileup bar plot depicting the cell abundance of each granulocyte subcluster.

(C) The comparison of c1 proportion between two groups in granulocytes.

(D) The comparison of c3 proportion between two groups in granulocytes.

(E) The comparison of c6 proportion between two groups in granulocytes.

(F) Dot plot exhibiting the *CXCL8* expression level of each individual in Gran c1.

(G–M) UMAP plots show the scaled mean AUC values of each pathway in granulocytes.

(N) Heatmap represents the scaled mean AUC values of differential signaling pathways in each subcluster. The clustering algorithm was applied to the row and column variables.

(O) Database and pathway names corresponding to each AUC number.

(P) Heatmap shows the scaled mean expression of differential genes in each subcluster. The clustering analysis was applied to the gene markers of the columns. All data were tested by independent sample t-test, and were represented as mean ± SEM.

of pro-inflammatory monocytes in plaque instability. Further analysis showed that *CXCL8+IL1B +* monocytes from CBMC (Mono c4) had a high degree of gene expression concordance with monocytes from plaques. Using the AUCell analysis, we quantified a specific gene set which included a list of characteristic genes of CXCL8+ inflammatory monocytes in atherosclerotic plaques identified by difference analysis (Table S9). The degree of enrichment of gene set across the designed groups (Figure 7G) and sub-clusters (Figure 7H) in CBMC monocytes was displayed and results showed that the upregulated genes within the plaques were most enriched in the Mono c4 cluster. In summary, CXCL8+IL1B+ monocytes in cord blood may be associated with pathogenic cell populations within atherosclerosis.

DISCUSSION

We present the first single-cell transcriptome atlas of CBMC derived from healthy or GDM affected mothers. Compared with children and adolescents, the proportion and transcriptome of monocytes in umbilical cord blood exhibited the most noticeable changes, with the least number of subsets with expression of proinflammatory-related pathways and highest number of cells with expression of proliferation-related pathways. Maternal GDM may reprogram fetal innate immune cells to a pro-inflammatory state, characterized by increased frequency of *CXCL8+IL1B +* monocytes and *CXCL8+FCGR3B +* neutrophils, along with enhanced cell-cell communications via the CXCL8-CXCR1/CXCR2 signaling pathway. Functional experiments of cord blood monocytes demonstrated heightened adhesion and phagocytosis capabilities in the GDM group. Notably, the transcriptional features of CXCL8+IL1B+ monocytes in cord blood were similar to those of coronary plaques myeloid cells from individuals with atherosclerotic cardiovascular disease. This insight offers a novel perspective on the increased long-term cardiovascular diseases risk associated with maternal GDM, illustrating the pro-inflammatory impact of the maternal GDM environment on fetal immune cells and providing new insights into potential mechanisms underlying enduring atherosclerosis risk from maternal GDM.

In our study, notable differences in both proportion and transcriptome of monocytes from umbilical cord blood were observed notable alterations when compared to those in peripheral blood from children and adolescents. This sheds light on developmental and functional differences in the immune system between these age groups. Existing research suggests heightened activity of the innate immune response during pregnancy, while the responses of adaptive immune cells are subdued.[24] The innate immune system acts as the initial line of defense, where monocytes, macrophages, and neutrophils play a crucial role in promptly recognizing and eliminating invading pathogens during fetal development, serving as the first defense against infections.[25] This nonspecific protection is especially vital during the fetal period when the immune system is not yet fully developed. Our study also confirmed weak pro-inflammatory abilities of monocytes in cord blood, albeit with increased differentiation and proliferation abilities. The weak pro-inflammatory abilities may indicate the adaptive process of the infant immune system to new environments and pathogens, aiming to shield infants from excessive inflammation. In this sense, the critical role of monocytes in fetal immunity should be addressed.

Despite the prevalent occurrence of GDM, research on its impact on neonatal immunity remains limited. Previous studies suggested that GDM can change T cell phenotype and increase the Th1/Th2 cytokine ratio of cord blood.[26,27] However, these studies primarily employed flow cytometry with limited markers, which did not comprehensively delineate the overall impact of GDM on neonatal immunity. Employing single-cell sequencing for the first time, we have shown that maternal GDM may activates the fetal innate immune response, characterized with an augmented frequency of CXCL8+IL1B+ monocytes and CXCL8+FCGR3B+ neutrophils in CBMC of GDM offspring. This might indicate a pro-inflammatory state in monocytes of GDM offspring, although the precise influence of these pro-inflammatory monocytes on the offspring remains elusive.

IL-8 and IL-1β, crucial pro-inflammatory cytokines, primarily regulate leukocyte migration and chemotaxis during inflammation and immune responses.[28] Our intercellular communication results revealed that CXCL8+IL1B+ monocytes in GDM offspring enhance interactions with neutrophils through the CXCL8-CXCR8 signaling pathway. Previous literature has indicated that CXCL8 contributes to inflammatory conditions like atherosclerosis.[29,30] Cohort studies have further confirmed a significantly elevated risk of atherosclerosis in GDM offspring.[31,32] Therefore, there is the possibility that GDM may promote atherosclerosis development in offspring by augmenting the pro-inflammatory state of monocytes in the cord blood. Interestingly, *in vitro* functional experiments demonstrated significantly enhanced phagocytic and adhesive capabilities in umbilical monocytes from the GDM group, and these functional alterations in monocytes are closely tied to atherosclerosis occurrence.[33] Importantly, the transcriptional features of CXCL8+IL1B+ monocytes in cord blood were similar to those of coronary

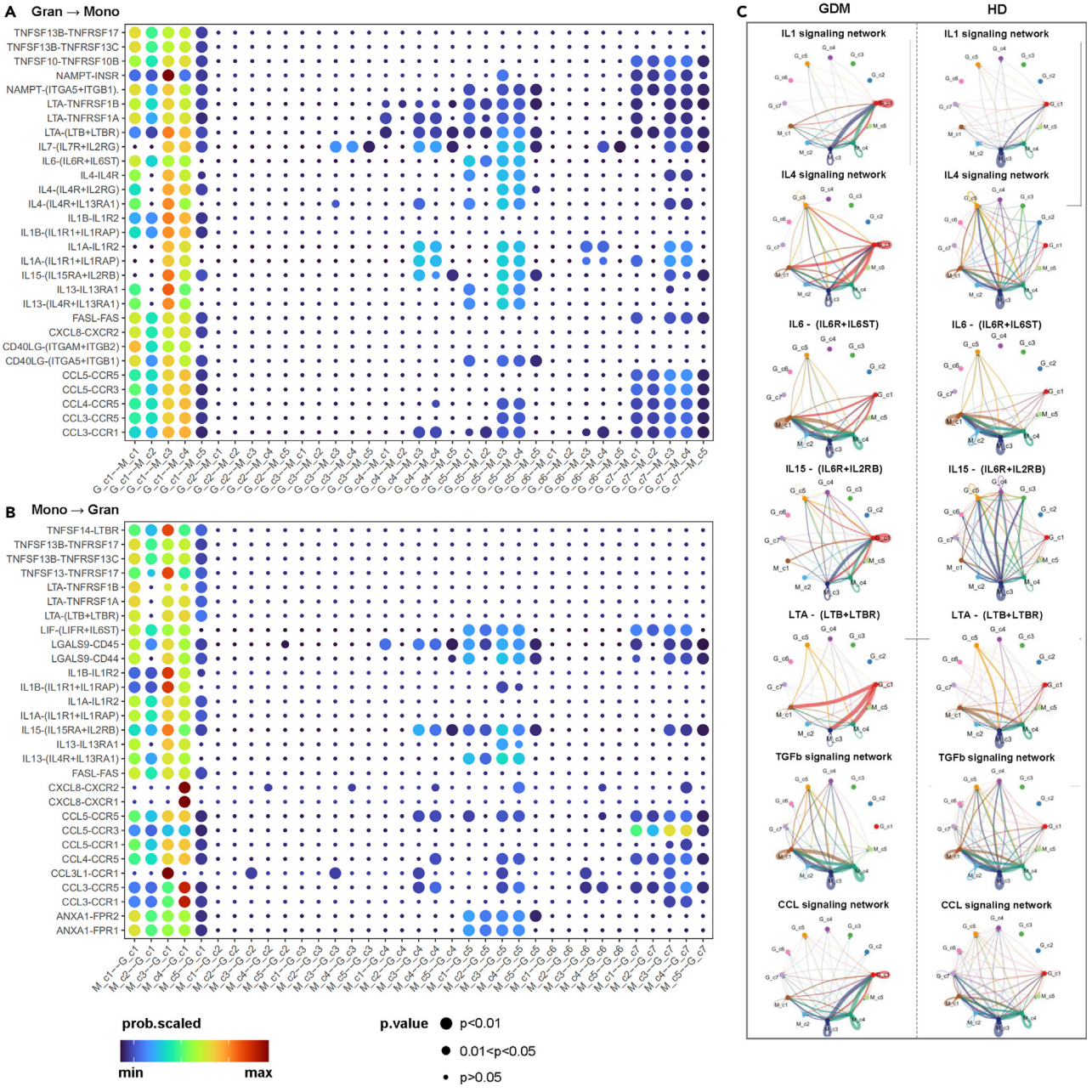

Figure 6. Cell-cell communications of CBMC monocytes and granulocytes

(A) Dot plot represents the communications between granulocytes (ligand provider) and monocytes (receptor provider). The size of the dots indicates the p value, and the color indicates the communication probability. Only signals with a mean communication probability of more than 1.00E-08 were displayed.

(B) Dot plot represents the communications between monocytes (ligand provider) and granulocytes (receptor provider). The dot size is inversely proportional to the p value. The color indicates the scaled mean communication probability. Higher probability suggests that the communication signaling is more enriched in the corresponding clusters.

(C) Circle plot shows the weight of statistically significant signaling interactions in GDM fetal CBMC compared to the control group.

plaques myeloid cells from individuals with atherosclerotic cardiovascular disease. This finding might establish a connection between GDM and inflammatory cells in coronary artery plaques, implying a long-term impact of maternal GDM on offspring, leading to the development of cardiovascular disease in adulthood. However, the specific mechanism remains unclear.

The intricate interplay of maternal GDM with fetal immunity necessitates a deeper understanding of their role in shaping long-term health outcomes. Numerous publications have demonstrated that maternal infection may shape the fetal immune system, increasing the risk of

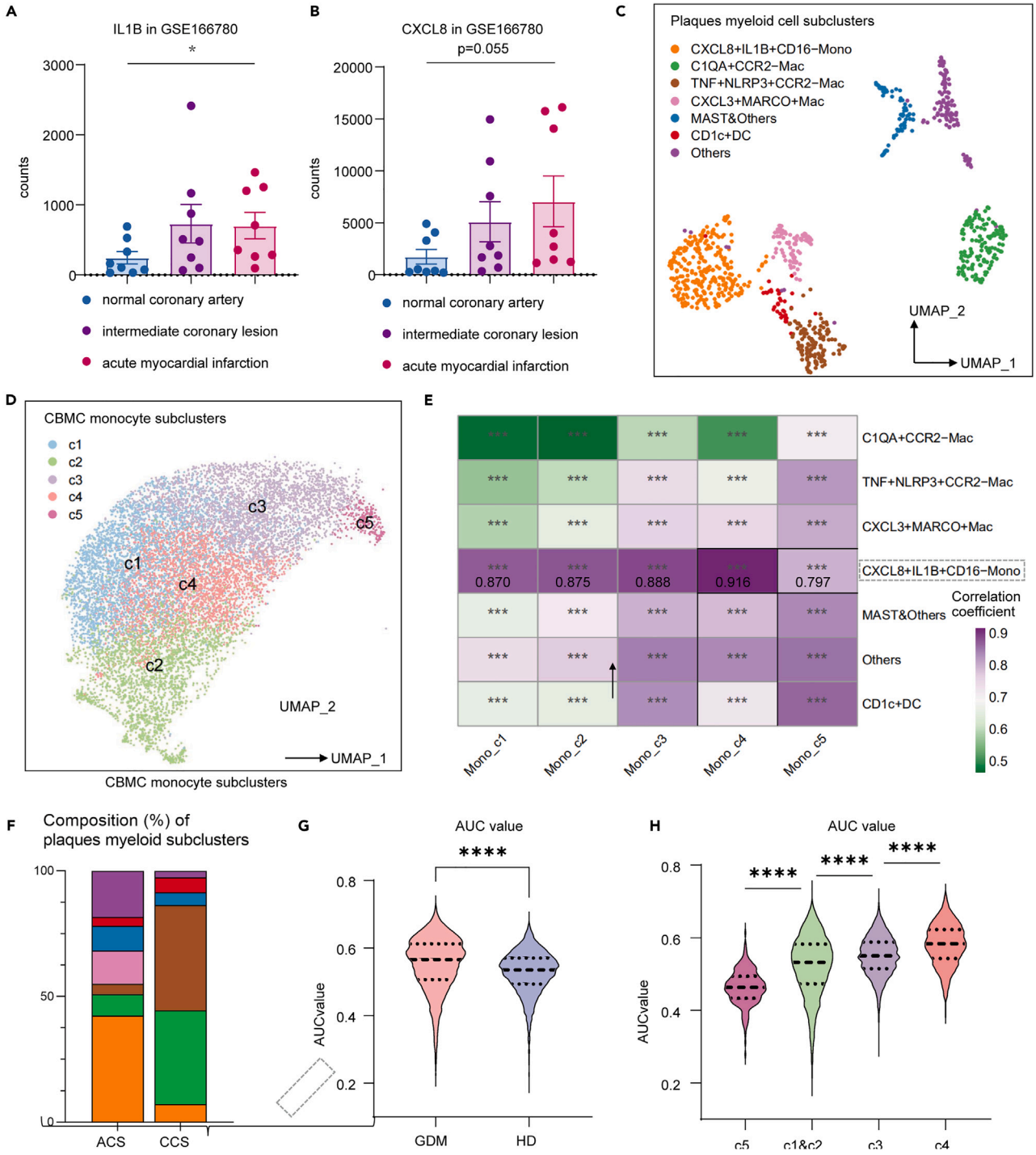

Figure 7. Combined analysis of CBMC monocytes and coronary plaques myeloid cells

(A and B) IL1B and CXCL8 expression pattern of peripheral blood monocytes in different stages of coronary artery disease (CAD) from a publicly available dataset by transcriptome sequencing.

(C) UMAP plots of myeloid cell subclusters in coronary culprit plaques.

(D) UMAP plots of monocyte subclusters in fetal CBMC.

(E) Heatmap shows the Pearson correlation coefficient in each subcluster. The correlation between monocyte subclusters in CBMC and monocytes in plaques was marked at the lower right.

(F) Pileup bar plot depicting the cell abundance of each myeloid cell subcluster in different plaques.

Figure 7. *Continued*

(G) In the data of acute atherosclerotic plaques, specifically highly expressed genes for *CXCL8+* inflammatory monocytes were chosen as the gene set that utilized to perform AUCell analysis for monocytes of cord blood. Violin plots highlight the AUC values in each designated group.

(H) Violin plots highlight the AUC values in each CBMC monocyte subcluster. Data were tested by independent sample t-test, and were represented as mean ± SEM. * means the p value of correlation analysis is <0.05. *** means the p value of correlation analysis is <0.001. **** means the p value of correlation analysis is <0.0001.

infections and autoimmune diseases in their offspring.[34–36] Prior studies have also indicated that fetal exposure to a diabetic intrauterine environment leads to the failure of cord blood endothelial progenitor cell adaptation.[15,37] Recent evidence demonstrates that hyperglycemia might induce trained immunity in macrophages and promote persistent pro-atherogenic characteristics.[21,38,39] These studies suggest that maternal GDM might induce immune training,[40] promoting increased CXCL8 and IL1B expression in offspring monocytes, leading to the occurrence of atherosclerosis in offspring in adulthood. This also suggests that CXCL8 and IL1B might serve as early intervention targets for preventing atherosclerosis in GDM offspring.

Our study demonstrated that maternal GDM might activate innate immunity, resulting in a pro-inflammatory state. The underlying mechanisms remain unclear. A possible hypothesis could be linked to elevated mild glucose intolerance, insulin resistance, and low-grade inflammation in GDM group.[41] In our study, CXCL8+IL1B+ monocytes from CBMCs were stimulated by high glucose *in vitro*. The positive correlation between the proportion of fetal CXCL8+IL1B+ monocytes and maternal glucose levels during pregnancy suggests that maternal mild hyperglycemia may create an adverse intrauterine environment, resulting in the pro-inflammatory state of fetal immune cells. We measured glucose and C-peptide levels in cord serum from mothers with GDM and matched healthy controls to explore potential factors. Despite similar cord blood glucose levels, fetal sera from mothers with GDM exhibited higher C-peptide levels (286.96 ± 132.42 vs. 178.39 ± 60.12 pmol/L in healthy group, $p = 0.045$), indicating a potential role of hyperinsulinemia, in addition to hyperglycemia, in the training process of fetal immunity.[42] Furthermore, previous research has shown that GDM mothers have elevated levels of various inflammatory factors such as IL-8, IL-1β, IL-6, and TLR2 in their placenta.[43,44] Whether GDM promotes an inflammatory state in the fetal umbilical cord blood through secondary inflammation resulting from maternal inflammation state needs further clarification. Previous studies have also indicated that accelerated gestational weight gain can influence DNA methylation patterns and adiposity in cord blood.[45,46] Recent research suggests that maternal obesity can weaken the antimicrobial response of fetal monocytes by affecting the chromatin accessibility of pro-inflammatory genes in umbilical cord monocytes, thereby increasing the risk of infections.[47] Whether GDM affects immune cells of offspring through epigenetic mechanisms such as DNA methylation and chromatin accessibility warrants further research.

In summary, our data provided the first single-cell transcriptomic atlas of CBMC, revealing that maternal GDM drives a pro-inflammatory state in neonatal monocytes and neutrophils immune cells, and that *CXCL8+IL1B +* monocytes might be promising targets for early intervention for atherosclerotic cardiovascular disease. These data may expand our understanding of maternal-fetal training immunity and atherosclerosis in adulthood, further supporting the DOHaD hypothesis.

Limitations of the study

First, the sample size of participants was relatively small, necessitating broader investigations to validate our findings. Second, a longitudinal approach involving serial sampling of the same patients over an extended period of time is recommended to elucidate the persistence of maternal GDM-induced trained immunity in atherosclerosis. Lastly, adequate functional experimental validation is needed for the impact of GDM on neonatal immunity and its implications for future atherosclerosis occurrence in the offspring. Ideally, *in vivo* and *ex vivo* experiments using specific cells and animals would provide more solid evidence. Isolation of IL1B + IL8+ monocytes for further investigation and *in vivo* transfusion are recommended for verifying the causal relationship.

STAR★METHODS

Detailed methods are provided in the online version of this paper and include the following:

- KEY RESOURCES TABLE
- RESOURCE AVAILABILITY
  - Lead contact
  - Materials availability
  - Data and code availability
- EXPERIMENTAL MODEL AND STUDY PARTICIPANT DETAILS
  - Human subjects
- METHOD DETAILS
  - External data
  - Sample collection and processing
  - Single-cell RNA sequencing experiment
  - Data processing and quality control for single-cell RNA sequencing
  - Dimension reduction and major cell type annotation

- Detection of differentially expressed genes
- PALMO
- Functional enrichment analysis
- AUCell analysis
- Cytotrace
- CellChat analysis
- Isolation and stimulation of monocytes
- Flow cytometry
- Phagocytosis and adhesion assay of monocytes

- QUANTIFICATION AND STATISTICAL ANALYSIS

SUPPLEMENTAL INFORMATION

Supplemental information can be found online at https://doi.org/10.1016/j.isci.2023.108637.

ACKNOWLEDGMENTS

We thank Dr. Jacques F Banchereau for providing the GEO dataset GSE135779, thank Dr. Chenxi Song for providing the GEO dataset GSE166780 and thank Dr. Ken-Ichi Hirata for providing the GEO dataset GSE184073. We thank Pro. Wen Deng for providing clinical information and sample collection of umbilical cord blood. We thank Yu Zhang for helping with sample collection and isolation.

Funding: This study was supported by the National Natural Science Foundation of China (grant no. 82070812), the Science and Technology Innovation Program of Hunan Province (2020RC4044), the Hunan Provincial Innovation Foundation for Postgraduate (grant no. CX20210363), and the Fundamental Research Funds for the Central Universities of Central South University (grant no. 2021zzts0361).

AUTHOR CONTRIBUTIONS

X.L. conceived and supervised the project. M.Y., and Y.Z. recruited subjects and performed the experiments. M.Y., Y.Z., and X.Y.L. performed bioinformatic analysis. M.Y., Y.Z., and X.Y.L. wrote the manuscript with inputs from S.S.L., J.H., and H.B.Y. X.L. revised the manuscript. All authors discussed and approved the manuscript submission.

DECLARATION OF INTERESTS

The authors declare no competing interests.

Received: August 10, 2023
Revised: October 18, 2023
Accepted: December 1, 2023
Published: December 5, 2023

REFERENCES

1. Zheng, Y., Ley, S.H., and Hu, F.B. (2018). Global aetiology and epidemiology of type 2 diabetes mellitus and its complications. Nat. Rev. Endocrinol. *14*, 88–98.
2. DeFronzo, R.A., Ferrannini, E., Groop, L., Henry, R.R., Herman, W.H., Holst, J.J., Hu, F.B., Kahn, C.R., Raz, I., Shulman, G.I., et al. (2015). Type 2 diabetes mellitus. Nat. Rev. Dis. Primers *1*, 15019.
3. Blüher, M. (2019). Obesity: global epidemiology and pathogenesis. Nat. Rev. Endocrinol. *15*, 288–298.
4. Oestreich, A.K., and Moley, K.H. (2017). Developmental and Transmittable Origins of Obesity-Associated Health Disorders. Trends Genet. *33*, 399–407.
5. Hanson, M.A., and Gluckman, P.D. (2014). Early developmental conditioning of later health and disease: physiology or pathophysiology? Physiol. Rev. *94*, 1027–1076.
6. Hoffman, D.J., Powell, T.L., Barrett, E.S., and Hardy, D.B. (2021). Developmental origins of metabolic diseases. Physiol. Rev. *101*, 739–795.
7. Chen, B., Du, Y.R., Zhu, H., Sun, M.L., Wang, C., Cheng, Y., Pang, H., Ding, G., Gao, J., Tan, Y., et al. (2022). Maternal inheritance of glucose intolerance via oocyte TET3 insufficiency. Nature *605*, 761–766.
8. Saravanan, P.; Diabetes in Pregnancy Working Group, Maternal Medicine Clinical Study Group, Royal College of Obstetricians and Gynaecologists, UK (2020). Gestational diabetes: opportunities for improving maternal and child health. The lancet. Diabetes & endocrinology *8*, 793–800.
9. McIntyre, H.D., Catalano, P., Zhang, C., Desoye, G., Mathiesen, E.R., and Damm, P. (2019). Gestational diabetes mellitus. Nat. Rev. Dis. Primers *5*, 47.
10. Zhang, C., and Catalano, P. (2021). Screening for Gestational Diabetes. JAMA *326*, 487–489.
11. Sweeting, A., Wong, J., Murphy, H.R., and Ross, G.P. (2022). A clinical update on Gestational Diabetes Mellitus. Endocr. Rev. *43*, 763–793.
12. Ye, W., Luo, C., Huang, J., Li, C., Liu, Z., and Liu, F. (2022). Gestational diabetes mellitus and adverse pregnancy outcomes: systematic review and meta-analysis. BMJ (Clinical research ed.) *377*, e067946.
13. Lowe, W.L., Jr., Scholtens, D.M., Kuang, A., Linder, B., Lawrence, J.M., Lebenthal, Y., McCance, D., Hamilton, J., Nodzenski, M., Talbot, O., et al. (2019). Hyperglycemia and Adverse Pregnancy Outcome Follow-up Study (HAPO FUS): Maternal Gestational Diabetes Mellitus and Childhood Glucose Metabolism. Diabetes Care *42*, 372–380.
14. Grunnet, L.G., Hansen, S., Hjort, L., Madsen, C.M., Kampmann, F.B., Thuesen, A.C.B., Granstrømi, C., Strøm, M., Maslova, E., Frikke-Schmidt, R., et al. (2017). Adiposity, Dysmetabolic Traits, and Earlier Onset of Female Puberty in Adolescent Offspring of Women With Gestational Diabetes Mellitus: A Clinical Study Within the Danish National Birth Cohort. Diabetes Care *40*, 1746–1755.
15. Gui, J., Rohrbach, A., Borns, K., Hillemanns, P., Feng, L., Hubel, C.A., and von Versen-Höynck, F. (2015). Vitamin D rescues dysfunction of fetal endothelial colony forming cells from individuals with gestational diabetes. Placenta *36*, 410–418.

16. Christoforou, E.R., and Sferruzzi-Perri, A.N. (2020). Molecular mechanisms governing offspring metabolic programming in rodent models of in utero stress. Cell. Mol. Life Sci. *77*, 4861–4898.
17. Howe, C.G., Cox, B., Fore, R., Jungius, J., Kvist, T., Lent, S., Miles, H.E., Salas, L.A., Rifas-Shiman, S., Starling, A.P., et al. (2020). Maternal Gestational Diabetes Mellitus and Newborn DNA Methylation: Findings From the Pregnancy and Childhood Epigenetics Consortium. Diabetes Care *43*, 98–105.
18. Zmora, N., Bashiardes, S., Levy, M., and Elinav, E. (2017). The Role of the Immune System in Metabolic Health and Disease. Cell Metab. *25*, 506–521.
19. Yanai, S., Tokuhara, D., Tachibana, D., Saito, M., Sakashita, Y., Shintaku, H., and Koyama, M. (2016). Diabetic pregnancy activates the innate immune response through TLR5 or TLR1/2 on neonatal monocyte. J. Reprod. Immunol. *117*, 17–23.
20. Roll, U., Scheeser, J., Standl, E., and Ziegler, A.G. (1994). Alterations of lymphocyte subsets in children of diabetic mothers. Diabetologia *37*, 1132–1141.
21. Edgar, L., Akbar, N., Braithwaite, A.T., Krausgruber, T., Gallart-Ayala, H., Bailey, J., Corbin, A.L., Khoyratty, T.E., Chai, J.T., Alkhalil, M., et al. (2021). Hyperglycemia Induces Trained Immunity in Macrophages and Their Precursors and Promotes Atherosclerosis. Circulation *144*, 961–982.
22. Thiem, K., Keating, S.T., Netea, M.G., Riksen, N.P., Tack, C.J., van Diepen, J., and Stienstra, R. (2021). Hyperglycemic Memory of Innate Immune Cells Promotes In Vitro Proinflammatory Responses of Human Monocytes and Murine Macrophages. J. Immunol. *206*, 807–813.
23. Lee, Y.S., Wollam, J., and Olefsky, J.M. (2018). An Integrated View of Immunometabolism. Cell *172*, 22–40.
24. Romero, R., Erez, O., Maymon, E., Chaemsaithong, P., Xu, Z., Pacora, P., Chaiworapongsa, T., Done, B., Hassan, S.S., and Tarca, A.L. (2017). The maternal plasma proteome changes as a function of gestational age in normal pregnancy: a longitudinal study. Am. J. Obstet. Gynecol. *217*, 67.e1–67.e21.
25. Zhang, Q., and Cao, X. (2021). Epigenetic Remodeling in Innate Immunity and Inflammation. Annu. Rev. Immunol. *39*, 279–311.
26. Seck, A., Hichami, A., Doucouré, S., Diallo Agne, F., Bassène, H., Ba, A., Sokhna, C., Khan, N.A., and Samb, A. (2018). Th1/Th2 Dichotomy in Obese Women with Gestational Diabetes and Their Macrosomic Babies. J. Diabetes Res. *2018*, 8474617.
27. Gomes Fagundes, D.L., França, E.L., da Silva Fernandes, R.T., Hara, C.d.C.P., Morceli, G., Honorio-França, A.C., and Calderon, I.d.M.P. (2016). Changes in T-cell phenotype and cytokines profile in maternal blood, cord blood and colostrum of diabetic mothers. J. Matern. Fetal Neonatal Med. *29*, 998–1004.
28. Li, Y., Huang, H., Liu, B., Zhang, Y., Pan, X., Yu, X.Y., Shen, Z., and Song, Y.H. (2021). Inflammasomes as therapeutic targets in human diseases. Signal Transduct. Target. Ther. *6*, 247.
29. Monaco, C., Gregan, S.M., Navin, T.J., Foxwell, B.M.J., Davies, A.H., and Feldmann, M. (2009). Toll-like receptor-2 mediates inflammation and matrix degradation in human atherosclerosis. Circulation *120*, 2462–2469.
30. Green, J.P., Souilhol, C., Xanthis, I., Martinez-Campesino, L., Bowden, N.P., Evans, P.C., and Wilson, H.L. (2018). Atheroprone flow activates inflammation via endothelial ATP-dependent P2X7-p38 signalling. Cardiovasc. Res. *114*, 324–335.
31. Yu, Y., Arah, O.A., Liew, Z., Cnattingius, S., Olsen, J., Sørensen, H.T., Qin, G., and Li, J. (2019). Maternal diabetes during pregnancy and early onset of cardiovascular disease in offspring: population based cohort study with 40 years of follow-up. BMJ (Clinical research ed.) *367*, l6398.
32. Tam, W.H., Ma, R.C.W., Ozaki, R., Li, A.M., Chan, M.H.M., Yuen, L.Y., Lao, T.T.H., Yang, X., Ho, C.S., Tutino, G.E., and Chan, J.C.N. (2017). Utero Exposure to Maternal Hyperglycemia Increases Childhood Cardiometabolic Risk in Offspring. Diabetes Care *40*, 679–686.
33. Björkegren, J.L.M., and Lusis, A.J. (2022). Atherosclerosis: Recent developments. Cell *185*, 1630–1645.
34. Apostol, A.C., Jensen, K.D.C., and Beaudin, A.E. (2020). Training the Fetal Immune System Through Maternal Inflammation-A Layered Hygiene Hypothesis. Front. Immunol. *11*, 123.
35. Huang, Q.Q., Tang, H.H.F., Teo, S.M., Mok, D., Ritchie, S.C., Nath, A.P., Brozynska, M., Salim, A., Bakshi, A., Holt, B.J., et al. (2020). Neonatal genetics of gene expression reveal potential origins of autoimmune and allergic disease risk. Nat. Commun. *11*, 3761.
36. Jacobsen, H., Walendy-Gnirß, K., Tekin-Bubenheim, N., Kouassi, N.M., Ben-Batalla, I., Berenbrok, N., Wolff, M., Dos Reis, V.P., Zickler, M., Scholl, L., et al. (2021). Offspring born to influenza A virus infected pregnant mice have increased susceptibility to viral and bacterial infections in early life. Nat. Commun. *12*, 4957.
37. Dincer, U.D. (2015). Fetal exposure to a diabetic intrauterine environment resulted in a failure of cord blood endothelial progenitor cell adaptation against chronic hypoxia. Stem Cells Cloning. *8*, 1–14.
38. Iida, J., Ishii, S., Nakajima, Y., Sessler, D.I., Teramae, H., Kageyama, K., Maeda, S., Anada, N., Shibasaki, M., Sawa, T., and Nakayama, Y. (2019). Hyperglycaemia augments lipopolysaccharide-induced reduction in rat and human macrophage phagocytosis via the endoplasmic stress-C/EBP homologous protein pathway. Br. J. Anaesth. *123*, 51–59.
39. Groh, L., Keating, S.T., Joosten, L.A.B., Netea, M.G., and Riksen, N.P. (2018). Monocyte and macrophage immunometabolism in atherosclerosis. Semin. Immunopathol. *40*, 203–214.
40. Sohrabi, Y., Godfrey, R., and Findeisen, H.M. (2018). Altered Cellular Metabolism Drives Trained Immunity. Trends Endocrinol. Metab. *29*, 602–605.
41. Johns, E.C., Denison, F.C., Norman, J.E., and Reynolds, R.M. (2018). Gestational Diabetes Mellitus: Mechanisms, Treatment, and Complications. Trends Endocrinol. Metab. *29*, 743–754.
42. Marcoux, S., Côté-Corriveau, G., Healy-Profitós, J., and Auger, N. (2022). Comment on Marcoux et al. Varying Impact of Gestational Diabetes Mellitus on Incidence of Childhood Cancers: An Age-Stratified Retrospective Cohort Study. Diabetes Care *45*, 1177–1183.
43. Stirm, L., Kovárová, M., Perschbacher, S., Michlmaier, R., Fritsche, L., Siegel-Axel, D., Schleicher, E., Peter, A., Pauluschke-Fröhlich, J., Brucker, S., et al. (2018). BMI-Independent Effects of Gestational Diabetes on Human Placenta. J. Clin. Endocrinol. Metab. *103*, 3299–3309.
44. Perichart-Perera, O., Muñoz-Manrique, C., Reyes-López, A., Tolentino-Dolores, M., Espino Y Sosa, S., and Ramírez-González, M.C. (2017). Metabolic markers during pregnancy and their association with maternal and newborn weight status. PLoS One *12*, e0180874.
45. Sharp, G.C., Lawlor, D.A., Richmond, R.C., Fraser, A., Simpkin, A., Suderman, M., Shihab, H.A., Lyttleton, O., McArdle, W., Ring, S.M., et al. (2015). Maternal pre-pregnancy BMI and gestational weight gain, offspring DNA methylation and later offspring adiposity: findings from the Avon Longitudinal Study of Parents and Children. Int. J. Epidemiol. *44*, 1288–1304.
46. Morales, E., Groom, A., Lawlor, D.A., and Relton, C.L. (2014). DNA methylation signatures in cord blood associated with maternal gestational weight gain: results from the ALSPAC cohort. BMC Res. Notes *7*, 278.
47. Sureshchandra, S., Doratt, B.M., Mendza, N., Varlamov, O., Rincon, M., Marshall, N.E., and Messaoudi, I. (2023). Maternal obesity blunts antimicrobial responses in fetal monocytes. Elife *12*, e81320.
48. Association, C.M. (2018). Chinese guideline for type 2 diabetes mellitus. Chin J Diabetes *38*, 292–344. (Chinese).
49. Nehar-Belaid, D., Hong, S., Marches, R., Chen, G., Bolisetty, M., Baisch, J., Walters, L., Punaro, M., Rossi, R.J., Chung, C.H., et al. (2020). Mapping systemic lupus erythematosus heterogeneity at the single-cell level. Nat. Immunol. *21*, 1094–1106.
50. Wang, C., Song, C., Liu, Q., Zhang, R., Fu, R., Wang, H., Yin, D., Song, W., Zhang, H., and Dou, K. (2021). Gene Expression Analysis Suggests Immunological Changes of Peripheral Blood Monocytes in the Progression of Patients With Coronary Artery Disease. Front. Genet. *12*, 641117.
51. Emoto, T., Yamamoto, H., Yamashita, T., Takaya, T., Sawada, T., Takeda, S., Taniguchi, M., Sasaki, N., Yoshida, N., Saito, Y., et al. (2022). Single-Cell RNA Sequencing Reveals a Distinct Immune Landscape of Myeloid Cells in Coronary Culprit Plaques Causing Acute Coronary Syndrome. Circulation *145*, 1434–1436.
52. Butler, A., Hoffman, P., Smibert, P., Papalexi, E., and Satija, R. (2018). Integrating single-cell transcriptomic data across different conditions, technologies, and species. Nat. Biotechnol. *36*, 411–420.
53. Becht, E., McInnes, L., Healy, J., Dutertre, C.A., Kwok, I.W.H., Ng, L.G., Ginhoux, F., and Newell, E.W. (2018). Dimensionality reduction for visualizing single-cell data using UMAP. Nat. Biotechnol. *37*, 38–44.
54. Squair, J.W., Gautier, M., Kathe, C., Anderson, M.A., James, N.D., Hutson, T.H., Hudelle, R., Qaiser, T., Matson, K.J.E., Barraud, Q., et al. (2021). Confronting false discoveries in single-cell differential expression. Nat. Commun. *12*, 5692.
55. Vasaikar, S.V., Savage, A.K., Gong, Q., Swanson, E., Talla, A., Lord, C., Heubeck, A.T., Reading, J., Graybuck, L.T., Meijer, P., et al. (2023). A comprehensive platform for analyzing longitudinal multi-omics data. Nat. Commun. *14*, 1684.

56. Aibar, S., González-Blas, C.B., Moerman, T., Huynh-Thu, V.A., Imrichova, H., Hulselmans, G., Rambow, F., Marine, J.C., Geurts, P., Aerts, J., et al. (2017). SCENIC: single-cell regulatory network inference and clustering. Nat. Methods *14*, 1083–1086.

57. GSEA Database. http://www.gsea-msigdb.org/gsea.

58. ggplot2 R Package. https://cran.r-project.org/web/packages/ggplot2/index.html.

59. Gulati, G.S., Sikandar, S.S., Wesche, D.J., Manjunath, A., Bharadwaj, A., Berger, M.J., Ilagan, F., Kuo, A.H., Hsieh, R.W., Cai, S., et al. (2020). Single-cell transcriptional diversity is a hallmark of developmental potential. Science *367*, 405–411.

60. Jin, S., Guerrero-Juarez, C.F., Zhang, L., Chang, I., Ramos, R., Kuan, C.H., Myung, P., Plikus, M.V., and Nie, Q. (2021). Inference and analysis of cell-cell communication using CellChat. Nat. Commun. *12*, 1088.

61. Bioinformatics. https://www.bioinformatics.com.cn.

STAR★METHODS

KEY RESOURCES TABLE

REAGENT or RESOURCE	SOURCE	IDENTIFIER
Antibodies		
PerCPCy5.5 anti-human CD14 antibody	BioLegend	Cat# 367110; RRID: AB_2566712
APC/Cyanine7 anti-human CD16 antibody	BioLegend	Cat# 302018; RRID: AB_314218
PE anti-human IL-8 antibody	BioLegend	Cat# 511408; RRID: AB_893465
AF647 anti-human IL-1β antibody	BioLegend	Cat# 508208; RRID: AB_604135
Chemicals, peptides, and recombinant proteins		
Lipopolysaccharides (LPS)	Solarbio	Cat#L8880
Dil-oxLDL	Yiyuan Biotechnologies	Cat#YB-002
Histopaque-1077	Sigma-Aldrich	Cat#10771-100ML
Brefeldin A	Sigma-Aldrich	Cat#B5936-200UL
Deposited data		
Single cell RNA-sequencing raw data for cord blood	GEO	GSE212309
Single cell RNA-sequencing raw data for child	GEO	GSE221297
A single cell approach to map cellular subsets involved in Systemic Lupus Erythematosus (SLE) heterogeneity	GEO	GSE135779
Gene expression analysis suggests immunological changes of peripheral blood monocytes in the progression of patients with coronary artery disease	GEO	GSE166780
Single Cell RNA Seq Reveals a Distinct Immune Landscape in Vulnerable Coronary Plaques.	GEO	GSE184073
Experimental models: Cell lines		
umbilical vein endothelial cells (HUV-EC-C, HUVEC)	Pro cell	Cat#CL-0122
Software and algorithms		
R	CRAN	https://www.r-project.org
Cell Ranger	10x Genomics	https://support.10xgenomics.com/
Seurat V3	Bioconductor	https://bioconductor.org/
edgeR	Bioconductor	https://bioconductor.org/
AUCell	Bioconductor	https://bioconductor.org/
CytoTRACE	Bioconductor	https://bioconductor.org/
CellChat	Bioconductor	https://bioconductor.org/
edgeR	Bioconductor	https://bioconductor.org/
PALMO	GitHub	https://github.com/
Critical commercial assays		
Zombie Aqua	BioLegend	Cat# 423101
CFSE reagent	Thermo Fisher	Cat#C34554
CD14 MicroBeads	Miltenyi	Cat#130-050-201

RESOURCE AVAILABILITY

Lead contact

Further information and requests for resources and reagents should be directed to and will be fulfilled by the lead contact, Xia Li (lixia@csu.edu.cn).

Materials availability

This study did not generate new unique reagents.

Data and code availability

- Single-cell RNA-seq data have been deposited at GEO and are publicly available as of the date of publication. Accession numbers are listed in the key resources table.
- This paper does not report original code.
- Any additional information required to reanalyze the data reported in this paper is available from the lead contact upon request.

EXPERIMENTAL MODEL AND STUDY PARTICIPANT DETAILS

Human subjects

This study was approved by the Research Ethics Committee of the Second Xiangya Hospital, Central South University (No.2016-021), and was conducted according to the Declaration of Helsinki guidelines. Written informed consent was obtained from all individuals. The peripheral blood was collected from three healthy children aged 1–10 years, between October 2020 and February 2021 for single-cell sequencing. Cord blood was donated by two cohorts recruited at the Second Xiangya Hospital, Central South University, between October and December 2020. Cohort I consisted of four GDM mothers and three healthy mothers for single-cell sequencing. Cohort II consisted of 12 GDM mothers and 13 healthy mothers for the *in vitro* validation experiment. The healthy control group was matched for maternal age, fetal sex, and pre-pregnancy BMI. All subjects were Han Chinese. GDM was diagnosed by an oral glucose tolerance test (OGTT, 75 g glucose) done at any time during pregnancy meeting at least one of the following criteria[48]: (1) 5.1 mmol/L $\leq$ fasting plasma glucose <7.0 mmol/L; (2) 1h glucose concentration $\geq$10.0 mmol/L; (3) 8.5 mmol/L $\leq$ OGTT 2h glucose <11.1 mmol/L. The inclusion criteria for the GDM group were as follows: (1) diagnosis of GDM; (2) no need for hypoglycemic agents to achieve satisfactory glycemic control; (3) singleton and full-term fetuses without malformation; (4) maternal pre-pregnancy BMI between 18.5 kg/m^2 and 27.9 kg/m^2. Pregnant participants with severe heart, liver, and kidney diseases, preeclampsia, pre-pregnancy diabetes, severe infection, drug use, smoking, or alcohol consumption were excluded.

METHOD DETAILS

External data

To discover the characteristics of immune cells in adolescent population, data on PBMC were downloaded from the GEO: GSE135779[49] dataset. To determine the gene expression characteristics of peripheral blood monocytes in different stages of patients with atherosclerosis, data on normal coronary artery, intermediate coronary lesion, and acute myocardial infarction were downloaded from the GEO: GSE166780[50] dataset. To determine the characteristics of monocytes in the plaques of patients with atherosclerosis, data on acute coronary syndrome (ACS) and chronic coronary syndrome (CCS) were downloaded from the GEO: GSE184073.[51] The above method was used to analyze the single-cell RNA sequencing data.

Sample collection and processing

Peripheral blood was collected in the morning before meals. Cord blood samples were collected from participants immediately after cesarean delivery to avoid the effects of stress on immune cells during vaginal birth. All samples were processed within 4 h of collection. Mononuclear cells were separated from the samples by density gradient centrifugation (Histopaque-1077, Sigma-Aldrich, USA), according to the manufacturer instructions. To be specific, whole blood was slowly spread on Histopaque-1077 with a density of 1.077 g/mL and centrifuged at 800g for 20 minutes. Both acceleration and deceleration were 0. The cell layer between Histopaque-1077 and plasma is absorbed as mononuclear cells. Fresh PBMC and CBMC from cohort I were immediately used for single-cell sequencing and CBMC from cohort II were frozen in 10% dimethyl sulfoxide/fetal bovine serum and deposited in liquid nitrogen after gradient freezing. The plasma from all cord blood samples was obtained by standard density gradient centrifugation. The concentrations of glucose, C-peptide, and lipids in the plasma were measured.

Single-cell RNA sequencing experiment

Cell density and viability were checked for fresh PBMC and CBMC from cohort I using Count Star (Alit life science, China), with cell viability >90% for each sample. Single-cell suspensions were transformed into barcoded single-cell RNA sequencing libraries using the Chromium Single-cell chip kit V3 and Chromium Single-cell 3′ Library and Gel Bead Kit V3(10× Genomics, USA). Single-cell cDNA synthesis and amplification were performed in a C1000 Touch Thermal Cycler (Bio Rad, USA). Finally, single-cell cDNA was sequenced using Illumina NovaSeq 6000.

Data processing and quality control for single-cell RNA sequencing

Raw FASTQ files were mapped to human reference GRCh38 using 10× Genomics Cell Ranger software suite (v.3.1.0).[52] Fastq sequence quality filtering and sequencing alignment were performed sequentially using the Cell Ranger pipeline. The gene barcode matrix from all samples was combined using the R package Seurat V3. Table S7 lists sequencing information for each sample. For quality control, only cells with 200–4500 genes and less than 15% of the mitochondrial genes were retained for subsequent analysis.

Dimension reduction and major cell type annotation

Highly variable genes were identified using the FindVariableFeatures function (default parameters). The RunPCA function in Seurat V3 was used to perform principal component analysis (PCA) on the top 2000 variable genes. Batch effects were removed using the R package Harmony version 1.0 based on the top 50 PCA components identified. The first 50 principal components were then used for cell clustering and Uniform Manifold Approximation and Projection (UMAP)[53] dimensional reduction. Cluster marker genes were recognized using the FindAllMarkers function, and clusters were manually annotated using known cell-type marker genes (Table S8).

Monocytes, granulocytes, T cells, B cells, and other immune cells were isolated from mononuclear cells for further sub-clustering. Following isolation, PCA and clustering were performed in the manner described in the dimension reduction and major cell type annotation section.

Detection of differentially expressed genes

Differential gene expression (DEG) testing was carried out in edgeR using EdgR-QLF.[54] DEGs were ranked by average log2 (fold change) after filtering with a minimum |log2(fold change) | of 0.585 and a maximum FDR (*q*-value) of 0.05.

PALMO

To discover how genes change with age, we performed PALMO (v0.1.2) analysis[55] based on the expression data in immune cell clusters annotated as monocytes.

Functional enrichment analysis

Gene Set EnrichmentAnalysis (GSEA) was performed using the OmicStudio tools, which can be found at https://www.omicstudio.cn/tool. Pearson correlation was utilized to assess the similarity of cell groups to identify similar functional subgroups.

AUCell analysis

To determine whether activation of certain pathways differs between cells, the AUCell R package[56] was utilized to calculate the degree of pathway activation for each cell using gene set enrichment analysis. The area under the curve (AUC) of gene expression in the selected pathway was calculated using a specific gene list downloaded from the GSEA database.[57] In the data of acute atherosclerotic plaques, specifically highly expressed genes were chosen as the distinct gene set for *CXCL8+* inflammatory monocytes (Table S9). This gene set was utilized to perform AUCell analysis for monocytes of cord blood. Cells that expressed more genes within the gene set had relatively high AUC values. Therefore, gene expression rankings for each cell were generated based on AUC value. The "AUCell_exploreThresholds" function was utilized to ascertain the threshold to recognize gene set active cells. To visualize the active clusters, the AUC score of each cell was mapped to the UMAP embedding using the ggplot2 R package (Version 3.3.5).[58]

Cytotrace

To predict the relative differentiation state of cells, we performed CytoTRACE (v0.1.0) analysis[59] based on the expression data in monocyte sub-clustering results.

CellChat analysis

CellChat[60] was utilized to investigate and visualize signaling pathway networks between different immune cells. First, the Seurat objects created using the preceding method were collated into CellChat objects using the "createCellChat" function. After annotating immune cells with relevant labels, their potential ligand-receptor interactions were deduced based on the expression of a receptor by one cell subtype and ligand expression by another. The "Cellchatdb. Human" database was used as a reference during this process. Finally, the figures were generated using the "netVisual_aggregate" function.

Isolation and stimulation of monocytes

Frozen CBMC were thawed, washed, and resuspended in complete culture medium (DMEM, 10% FBS, and 1% penicillin/streptomycin). Monocytes were then enriched by magnetic cell sorting using $CD14^+$ magnetic beads (Miltenyi Biotec, Germany), according to the manufacturer instructions. Monocytes were cultured in DMEM containing normal (5.5 mmol/L) or high glucose (25.0 mmol/L) at a density of 10^5 cells per well in 12-well plates. Brefeldin A (BFA, Sigma-Aldrich, USA) was added to the medium after incubation for 24 h. Monocytes were then treated with or without 1 ng/mL LPS (Solarbio, China) for 5 h until analysis.

Flow cytometry

Monocytes were stained with fluorescently-labeled monoclonal antibodies (PerCPCy5.5 anti-human CD14 antibody (BioLegend Cat# 367110, RRID: AB_2566712), APC/Cyanine7 anti-human CD16 antibody (BioLegend Cat# 302018, RRID:AB_314218), PE anti-human IL-8 antibody (BioLegend Cat# 511408, RRID:AB_893465), AF647 anti-human IL-1β antibody (BioLegend Cat# 508208, RRID:AB_604135), and Zombie Aqua (BioLegend Cat# 423101). Flow cytometry was performed using the standard surface and intracellular cytokine staining protocols.

Stained monocytes were detected using a spectral flow cytometer (Cetek NL3000). Only live cells were used for the analysis based on the Zombie Aqua staining. At least 100,000 cells in the monocytes gate were collected by flow cytometer and then analyzed with FlowJo version 10.0 software (Tree Star, Inc., Ashland, USA). The mean fluorescence intensity of IL-8 and IL-1β in the monocytes gate was calculated. The experiment was repeated twice under the same conditions. Scatter diagrams were plotted by bioinformatics,[61] an online data analysis, and visualization platform.

Phagocytosis and adhesion assay of monocytes

Monocytes from umbilical cord blood were enriched by magnetic cell sorting using CD14 MicroBeads (Miltenyi Biotec, Germany) and seeded at 2×10^5 cells per milliliter in 48-well plates, with three replicates for each sample. For phagocytosis assay, monocytes were incubated with 40 μg/mL red fluorescence-labeled Dil-oxLDL (Yiyuan Biotechnologies, China) at 37°C for 3 h. The samples were then examined under a fluorescence microscope, with five images acquired per well. The percentage uptake was calculated as the number of red fluorescence-labeled monocytes divided by the total number of monocytes.

For adhesion assay, monocytes were fluorescently labeled green using the CFSE reagent (Thermo Fisher Scientific, USA) at 5μM according to the manufacturer instructions. The labeled monocytes were then added to a 48-well plate at a density of 5×10^4 cells per milliliter for 5 h at 37°C. The 48-well plate was covered with umbilical vein endothelial cells (Pro cell, China) at the bottom of each well. The number of adhered cells was recorded and averaged with five images per well acquired under a fluorescence microscope. The average number of fluorescently labeled cells in each field of view reflected the adhesion capacity of mononuclear cells to umbilical vein endothelial cells. These experiments were repeated twice under the same conditions. The ImageJ software was used to adjust the brightness of the displayed images equally.

QUANTIFICATION AND STATISTICAL ANALYSIS

Statistical analyses were performed using R Studio, GraphPad Prism 8, and IBM SPSS Statistics 22. Data were expressed as mean ± standard error (mean +SEM) unless otherwise stated. Measurement data with normal distribution were tested by independent sample t-test. Kruskal-Wallis one-way ANOVA was used for non-normally distributed data. p-values less than 0.05 were considered statistically significant (*$p < 0.05$, **$p < 0.01$, ***$p < 0.001$, ****$p < 0.0001$).